GEOCHRONOMETRIA 52 (2025) 200791
DOI 10.20858/geochr/200791

Available online at https://www.geochronometria.com/

DOSE RATE MEASUREMENTS WITH CORRELATED U, Th AND K UNCERTAINTIES USING FULL NaI:Tl GAMMA SPECTRUM ANALYSIS

MACIEJ GOSEK[1], MAKSYMILIAN JĘDRZEJOWSKI[1], GRZEGORZ PORĘBA[1], KACPER KŁOSOK[1], TOMASZ BŁACHOWICZ[1] and KONRAD TUDYKA[1]

[1] Silesian University of Technology, Institute of Physics – Centre for Science and Education, Konarskiego 22B, 44-100 Gliwice, Poland

Received 10 June 2024 Accepted 4 February 2025

Abstract
This study introduces a new method for measuring uranium, thorium decay chains, and ^{40}K in geological materials using NaI:Tl gamma spectrometry. The novel approach involves fitting data to model reference spectra via custom software, processing full mixed spectra to estimate pure component spectra quantifying radionuclides concentrations and evaluating their correlations. These correlations are crucial in calculating environmental dose rates for trapped charge dating. The methodology was validated using a Canberra InSpector 1000 spectrometer, with results cross-checked against high-resolution gamma spectrometry. With the use of the µRate web application, dose rates uncertainties were lowered by including correlated inputs, which results in improved precision in trapped charge dating.

Keywords
NaI:Tl, gamma spectrometry, environmental radioactivity, trapped charge dating, dose rate, radioactive materials

1. Introduction

Trapped Charge Dating (TCD) includes various techniques like Optically Stimulated Luminescence (OSL), Thermoluminescence (TL), and Electron Spin Resonance (ESR), and is frequently employed in earth sciences and archaeology to calculate ages based on equivalent doses and dose rates (Adamiec, 2005a, 2005b; Bejarano-Arias *et al.*, 2023; Bluszcz and Adamiec, 2006; Brill *et al.*, 2022; Ginter *et al.*, 2022; Moska *et al.*, 2019; Panin *et al.*, 2017; Perić *et al.*, 2022; Sontag-González *et al.*, 2021). The dose rate arises from the uranium and thorium decay chains and ^{40}K and usually to a lesser extent from cosmic rays. Those radionuclides in environmental materials are frequently measured by means of gamma spectrometry (Murray *et al.*, 2015; Bonczyk, 2018; Murray *et al.*, 2018; Michalik *et al.*, 2020). Due to low environmental radionuclides concentrations, the measurements are time-consuming and shortening the measurement time will limit the dose rate precision and, consequently age precision.

To detect gamma radiation in the field or in collected samples, thallium doped sodium iodide (NaI:Tl) scintillators are used. Such a scintillator is coupled to a photomultiplier tube which converts the photons originating from scintillations into electrical signals. The interactions giving rise to scintillations include the photoelectric effect, the Compton effect, and pair production. The photoelectric effect gives peaks in spectrum that are characteristic for specific radionuclides (Bonczyk, 2018; Mauz *et al.*, 2022; Murray *et al.*, 2018; Arnold *et al.*, 2012) that allows radionuclide identification and radioactivity concentration measurements.

In some works, a signal beyond photopeaks is analysed (Bu *et al.*, 2018, 2021; Duval and Arnold, 2013; Hendriks *et al.*, 2001; Kumar *et al.*, 2022; Mercier and Falguères, 2007; Rhodes and Schwenninger, 2007). Those methods analyse not only the photoelectric effect, i.e. the photopeaks, but also the entire range of electron energies created by the Compton effect and by pair production. This has the advantage of providing better count rate statistics when compared to analyzing peaks when only certain

Corresponding author: M. Gosek
e-mail: macigos598@student.polsl.pl

ISSN 1897-1695 (online), 1733-8387 (print)

narrow fragments of spectrum are analyzed. Full spectra analysis is therefore an alternative that allows shortening the measurement time.

In this work we aim to investigate how full spectrum analysis can improve the dose rate precision measured in environmental materials for TCD, by taking into account correlations that arise when estimating the uranium decay chain, thorium decay chain, and ^{40}K activity concentration.

2. Experimental section

2.1. System construction

The investigated system is based on a portable gamma NaI:Tl spectrometer scintillation detector InSpector 1000 manufactured by Canberra Industries, Inc. with 2" × 2" NaI:Tl probe. The detector and the sample chamber are inside a passive shield that is built from high purity copper and old lead with thicknesses of about 5 mm and 10 cm, respectively. The internal volume was kept as small as possible to minimise the influence of ^{222}Rn daughter nuclides decaying in the measurement chamber. Schematic cross-section and block diagram are provided in **Fig. 1**.

Before and during each measurement, the system was kept in an air-conditioned laboratory at 20–22 °C and 30–40% relative humidity. This was done to minimize temperature drift correction (Bu *et al.*, 2018).

2.2. System calibration and measurement setup

The system was calibrated using reference materials from the International Atomic Energy Agency (IAEA), namely IAEA-RGU-1, IAEA-RGTh-1, and IAEA-RGK-1. The IAEA-RGU-1 and IAEA-RGTh-1 were prepared by the Canada Centre for Mineral and Energy Technology. These standards originated from a uranium ore named BL-5 and a thorium ore called OKA-2, respectively. To create these standards, the raw materials from these ores were diluted with silica powder that had minimal uranium and thorium concentrations. Due to the geological source of the material and information from the IAEA, the decay chains in these reference materials are assumed to be in secular equilibrium with their parent activity concentration. The IAEA-RGK-1 standard was produced using high-purity potassium sulphate (99.8%). Another reference material was created by mixing IAEA-RGU-1, IAEA-RGTh-1, and IAEA-RGK-1 by equal weights. **Table 1** contains the recommended radionuclide concentrations in IAEA-RGU-1, IAEA-RGTh-1, and IAEA-RGK-1 certified reference materials, which are used for calibration.

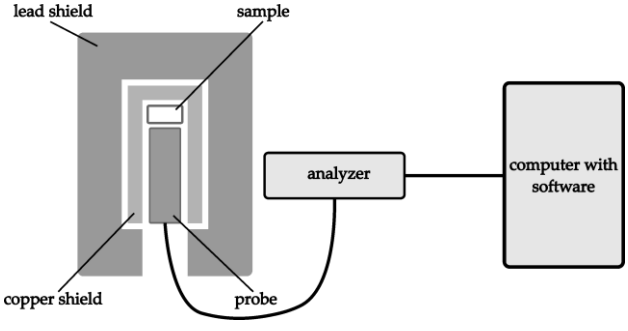

Fig. 1. *Schematic cross section and block diagram of the gamma spectrometer system.*

Each of the reference and test samples was dried, and 100 mL of granular material was placed in a separate γBeaker container and sealed. The γBeaker containers effectively prevent ^{222}Rn leakage, with a leakage rate close to 0% (Poręba *et al.*, 2020; Tudyka *et al.*, 2021). Before measurements, all samples were weighed. Subsequently, reference and test samples were stored for about 30 days to obtain secular equilibrium to avoid bias arising from ^{222}Rn emanation (Markkanen and Arvela, 1992; Sakoda *et al.*, 2010, 2011; Seo *et al.*, 2001). The background was measured using an empty γBeaker container.

2.3. Spectra processing and deconvolution

The obtained spectra are saved in a file with a *.CNF extension (Canberra Nuclear File) and transferred to a computer. Next, a program written specifically for this study reads them. For reading CNF files, an implementation from the project 'CNFreader' on GitHub (Condori, 2020) was used, also allowing saving of the read values into a text file.

To avoid channels without counts that would bias the fitting and to reduce the computation time, each spectrum is reduced from 1024 channels to 64 channels by summing counts from 16 consecutive channels. The program loads the reduced spectra from both the background and reference materials, followed by the reading of unknown sample spectra.

As input data, $L + 1$ reference materials with known U decay chain, Th decay chain, and ^{40}K are collected. At least

Table 1. *Recommended radionuclide concentrations in IAEA-RGU-1, IAEA-RGTh-1, and IAEA-RGK-1 certified reference materials used for spectrometer calibration. Reference values were converted to Bq kg^{-1}, assuming an abundance of 99.28% ^{238}U. Uncertainties are expressed as 1σ.*

name	^{238}U activity concentration, (Bq·kg^{-1})		^{232}Th activity concentration, (Bq·kg^{-1})		^{40}K activity concentration, (Bq·kg^{-1})	
	value	uncertainty	value	uncertainty	value	uncertainty
IAEA-RGTh-1	78	6	3250	180	6.3	3.2
IAEA-RGU-1	4941	99	< 0.63	N/A	< 4	N/A
IAEA-RGK-1	< 0.01	N/A	< 0.04	N/A	14180	160

three of them need to contain linearly independent U decay chain, Th decay chain, and ^{40}K concentrations. Those spectra are stored in the form of row vectors consisting of count rates (N) in consecutive channels in s^{-1} as follows:

$$_{M,0}\mathbf{N}_R = [_{M,0}N_{R,0},\ _{M,0}N_{R,1},\ \ldots,\ _{M,0}N_{R,63}], \quad (1a)$$

...,

$$_{M,L}\mathbf{N}_R = [_{M,L}N_{R,0},\ _{M,L}N_{R,1},\ \ldots,\ _{M,L}N_{R,63}], \quad (1b)$$

where $_{M,0}\mathbf{N}_R$ denotes the first reference material, and $_{M,L}\mathbf{N}_R$ the last. At least three linearly independent reference materials need to be used for calibration.

In addition, the measured background spectra are stored in the same form:

$$_M\mathbf{N}_{BG} = [N_{BG,0},\ N_{BG,1},\ \ldots,\ N_{BG,63}]. \quad (2)$$

Similarly, for each concentration, that is, U decay chain, Th decay chain, and ^{40}K, the three pure theoretical corresponding spectra $_{T,Th}\mathbf{M}$, $_{T,U}\mathbf{M}$, and $_{T,K}\mathbf{M}$ are defined, where each term is expressed in s^{-1}/ (Bq kg^{-1}). Those three theoretical spectra are corresponding pure U decay chain or Th decay chain or ^{40}K. Three pure theoretical they are stored in the form of row vectors consisting of count rates in consecutive channels:

$$_{T,Th}\mathbf{M} = [_{T,Th}M_0,\ _{T,Th}M_1,\ \ldots,\ _{T,Th}M_{63}], \quad (3a)$$

$$_{T,U}\mathbf{M} = [_{T,U}M_0,\ _{T,U}M_{1,\ldots},\ _{T,U}M_{63}], \quad (3b)$$

$$_{T,K}\mathbf{M} = [_{T,K}M_0,\ _{T,K}M_1,\ \ldots,\ _{T,K}M_{63}]. \quad (3c)$$

Next, we form the residual sums of reference materials

$$_{R,0}\mathbf{RS} = {}_{M,0}\mathbf{N}_R - ({}_{T,Th}\mathbf{M} \cdot {}_{Th}A_{R,0} \cdot f_{R,0} + {}_{T,U}\mathbf{M} \cdot {}_{U}A_{R,0} \cdot f_{R,0} + {}_{T,K}\mathbf{M} \cdot {}_{K}A_{R,0} \cdot f_{R,0} + {}_M\mathbf{N}_{BG}), \quad (4a)$$

...,

$$_{R,L}\mathbf{RS} = {}_{M,L}\mathbf{N}_R - ({}_{T,Th}\mathbf{M} \cdot {}_{Th}A_{R,L} \cdot f_{R,L} + {}_{T,U}\mathbf{M} \cdot {}_{U}A_{R,L} \cdot f_{R,L} + {}_{T,K}\mathbf{M} \cdot {}_{K}A_{R,L} \cdot f_{R,L} + {}_M\mathbf{N}_{BG}) \quad (4b)$$

and unknown sample

$$_S\mathbf{RS} = {}_M\mathbf{N}_S - ({}_{T,Th}\mathbf{M} \cdot {}_{Th}A \cdot f_s + {}_{T,U}\mathbf{M} \cdot {}_{U}A \cdot f_s + {}_{T,K}\mathbf{M} \cdot {}_{T,K}A \cdot f_s + {}_M\mathbf{N}_{BG}). \quad (5)$$

Where $_{Th}A_{R,0}$, $_{U}A_{R,0}$ and $_{K}A_{R,0}$ represent thorium, uranium and potassium radioactivity concentration (Bq kg^{-1}) in first reference material, respectively. Similarly, $_{Th}A_{R,L}$, $_{U}A_{R,L}$ and $_{K}A_{R,L}$ correspond to the last reference material measured. Next, the masses are normalized with f terms. Finally, $_{Th}A_{R,0}$, $_{U}A_{R,0}$ and $_{K}A_{R,0}$ are respectively thorium, uranium and potassium radioactivity concentration (Bq kg^{-1}) in an unknown sample.

Then the weighted residual sum of squares is minimised

$$\text{argmin}(\sum({}_{R,i}\mathbf{RS} \odot {}_{R,i}\mathbf{W})({}_{R,i}\mathbf{RS} \odot {}_{R,i}\mathbf{W})^T + ({}_S\mathbf{RS} \odot {}_S\mathbf{W})({}_S\mathbf{RS} \odot {}_S\mathbf{W})^T) \quad (6)$$

by adjusting arguments $_{Th}A$, $_{U}A$, $_{K}A$ of radionuclide concentration as well as three pure theoretical net spectra $_{T,Th}\mathbf{N}$, $_{T,U}\mathbf{N}$ and $_{T,K}\mathbf{N}$. The symbol "⊙" represents the element-wise product, also known as the Hadamard product. $_{R,i}\mathbf{W}$ = [$_{R,i}\sigma_0^{-1}$, $_{R,i}\sigma_1^{-1}$, …, $_{R,i}\sigma_{63}^{-1}$] and $_S\mathbf{W}$ = [$_S\sigma_0^{-1}$, $_S\sigma_1^{-1}$, …, $_S\sigma_{63}^{-1}$] are row vectors of Poisson uncertainties in corresponding channels of measured reference materials and unknown samples. This step is done using the Trust Region Reflective algorithm (Branch *et al.*, 1999). In addition, the covariance matrix is estimated based on a linear approximation to the model function around the optimum (Vugrin *et al.*, 2007). This operation is implemented in Python using NumPy (Harris *et al.*, 2020) and SciPy (Virtanen *et al.*, 2020) libraries. The covariance matrix is used to determine how the radioactivities of thorium, uranium, and potassium vary in relation to one another.

Fitting is concentrated on the central part of the spectrum, because the low as well as the high energy parts of the spectrum do not contain useful and stable information (Kumar *et al.*, 2022; Mercier and Falguères, 2007). In our study, we used the 770-2900 keV range, where curve fitting described both, the reference spectra as well as the unknown sample spectra, well.

In summary this allows us to perform spectra deconvolution into pure U decay chain, Th decay chain, and ^{40}K, assess radioactivity concentrations and their covariance matrix. After spectra deconvolution each theoretical spectrum $_{T,Th}\mathbf{M}$, $_{T,U}\mathbf{M}$ and $_{T,K}\mathbf{M}$ is scaled by the corresponding radioactivity $_{Th}A$, $_{U}A$ and $_{K}A$ so that after adding the background spectrum $_M\mathbf{N}_{BG}$ we obtain the best possible match with our measured spectrum. This effectively allows us to retrieve radioactivity concentrations $_{Th}A$, $_{U}A$ and $_{K}A$ and how those radioactivity concentrations can change with relatives to each other.

2.4. Dose rate calculations

In TCD, radionuclide concentration is used to calculate the environmental dose rate received by natural dosimeters such as quartz or feldspar. Apart from the radionuclide concentration, this environmental dose rate depends on several factors, including the size of the natural dosimeters, water content, and the so-called *a*-value, which accounts for the differing luminescence response to alpha and beta particles. In this study, we investigated dose rate calculations for arbitrarily chosen parameters that frequently appear in such contexts. To estimate dose rates we used values that are typically used in luminescence dating (Ginter *et al.*, 2022; Pawełczyk *et al.*, 2023). We drew 50000 random radionuclide concentrations i.e. ^{238}U, ^{232}Th decay chains, and ^{40}K from a multivariate normal distribution using a covariance matrix from fitting. Next, the ^{238}U, ^{232}Th decay chains, and ^{40}K concentrations were converted to dose rates using values provided by Cresswell *et al.* (2018). The a-value is used to account for different interactions of α particles with matter (Aitken, 1985a) and was set to 0.04 ± 0.02 (Lai *et al.*, 2008). Water content was assumed to be 10 ± 5% (Aitken, 1985b; Aitken and Xie, 1990). Such

values are frequently reported in TCD of geological sediments. Next, fraction correction for 90–125 μm grains was applied following Brennan *et al.* (1991) and Guérin *et al.* (2012). Calculations were performed in the μRate web app which can include covariances of radionuclides (Tudyka *et al.*, 2023). The detailed calculation procedure was published earlier (Tudyka *et al.*, 2023). Accounting for correlated results is expected to enhance the precision of the obtained results (Rocznik *et al.*, 2023; Tudyka *et al.*, 2020).

The algorithm described was tested using the following reference materials: IAEA-RGU-1 (**Fig. 2**), IAEA-RGK-1 (**Fig. 3**) and IAEA-RGTh-1 (**Fig. 4**). Background measurements were also taken (**Fig. 5**). The radionuclide concentrations in the artificial reference material, labelled as MIX (**Fig. 6**), estimated by the developed software, was found to be in perfect agreement with the known concentration (one third of each of the reference materials).

2.5. Materials and measurements

All measurements were conducted using a gamma radiation spectrometer equipped with a scintillation detector InSpector 1000 manufactured by Canberra, which is typically used as a portable spectrometer for field measurements of activity. Once calibrated, it can be used in arbitrary conditions, in the field or in a laboratory, to determine the activity of natural radionuclides for the uranium, thorium series, and ^{40}K. For this purpose, it is sometimes used to determine dose rates during luminescence dating of rocks and sediments (Moska *et al.*, 2021).

The average measurement time was 24 hours, and the number of channels was equal to 1024. We analyzed nine sediment samples from two locations. The first series, labeled 'JB,' comprised six clay sediment samples. The sec-

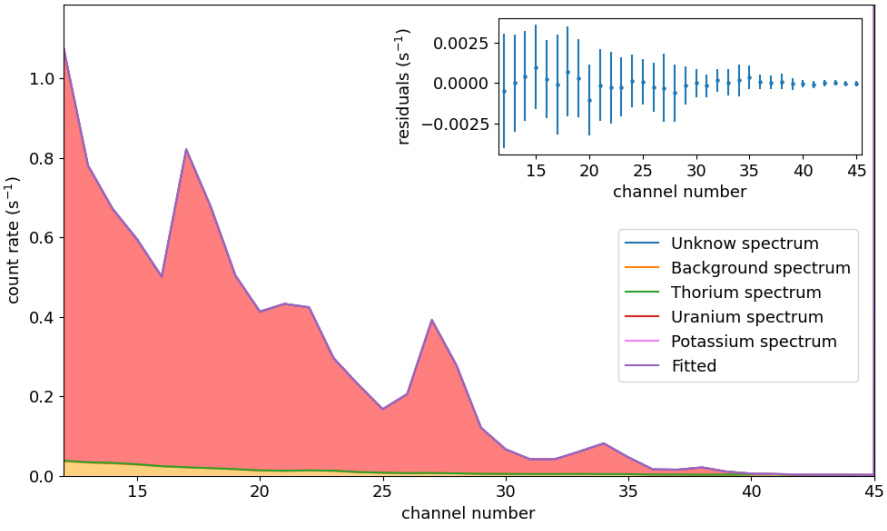

Fig. 2. *Reference material spectra processed and decomposed by the proposed algorithm for RGU-1. An unknown spectrum (blue line) was matched to a fitted spectrum (purple line), from which background (orange line), thorium (green line), uranium (red line), and potassium (pink line) were calculated. Residuals of the fitted spectra deconvolution are shown in inset.*

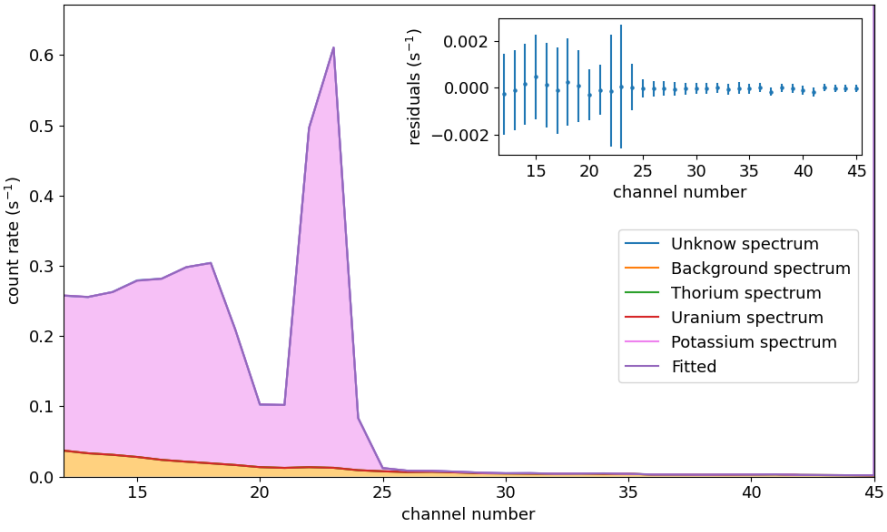

Fig. 3. *Reference material spectra processed and decomposed by the proposed algorithm for: RGK-1. An unknown spectrum (blue line) was matched to a fitted spectrum (purple line), from which background (orange line), thorium (green line), uranium (red line), and potassium (pink line) were calculated. Residuals of the fitted spectra deconvolution are shown in inset.*

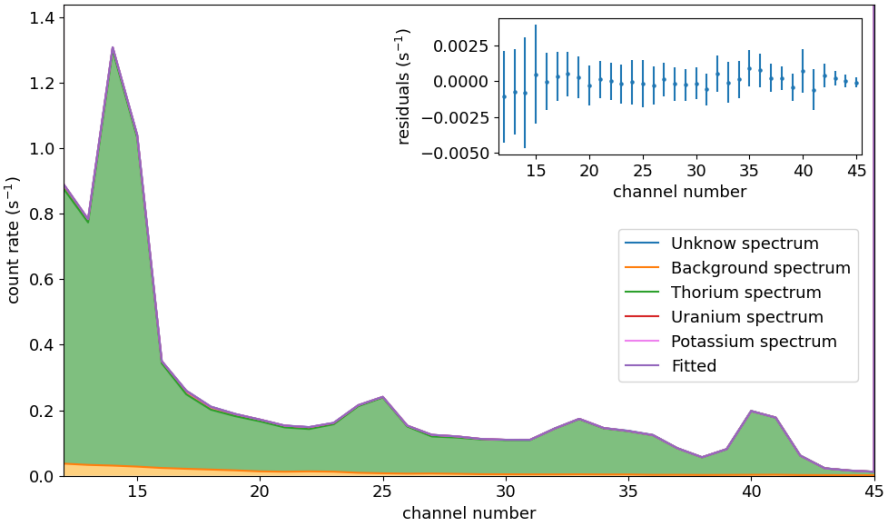

Fig. 4. *Reference material spectra processed and decomposed by the proposed algorithm for RGTh-1. An unknown spectrum (blue line) was matched to a fitted spectrum (purple line), from which background (orange line), thorium (green line), uranium (red line), and potassium (pink line) were calculated. Residuals of the fitted spectra deconvolution are shown in inset.*

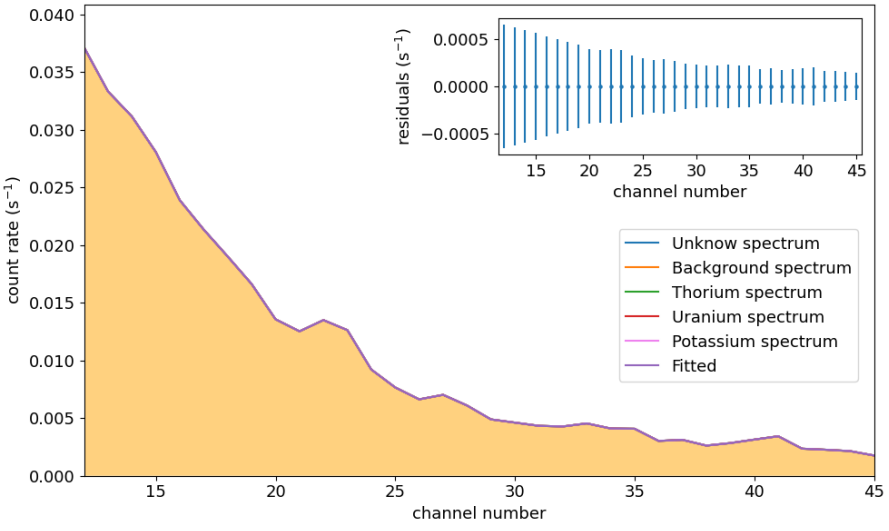

Fig. 5. *Reference material spectra processed and decomposed by the proposed algorithm for the background sample. An unknown spectrum (blue line) was matched to a fitted spectrum (purple line), from which background (orange line), thorium (green line), uranium (red line), and potassium (pink line) were calculated. Residuals of the fitted spectra deconvolution are shown in inset.*

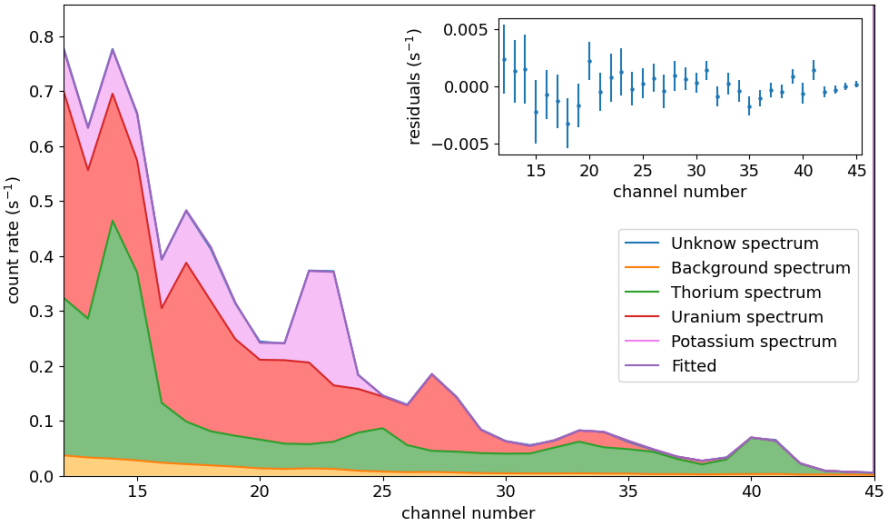

Fig. 6. *Reference material spectra processed and decomposed by the proposed algorithm for a 1 : 1 : 1 mixture of RGK-1, RGTh-1, and RGU-1, labeled as MIX. An unknown spectrum (blue line) was matched to a fitted spectrum (purple line), from which background (orange line), thorium (green line), uranium (red line), and potassium (pink line) were calculated. Residuals of the fitted spectra deconvolution are shown in inset.*

ond series, labeled 'OSL/REP', included three dolomite limestone samples collected from depressions at a historical mining site in Poland. All measurements, calibrations, and sample analyses were conducted using the setup shown in **Fig. 1**. Test sample activity concentrations were mass normalised to match the mass of the reference materials.

2.6. High Resolution Gamma Spectrometry

For comparative analysis, we used a High-Resolution Gamma Spectrometer (HRGS) equipped with Extended-Range Germanium Detectors, model GX 4018, supplied by Canberra Industries, Inc. This detector was interfaced with a DSA 1000 pulse analyser, also from Canberra Industries, Inc. Data analysis was conducted using the Genie 2000 software, provided by the same company. The calibration of the HRGS was done using the IAEA-RGU-1, IAEA-RGTh-1, and IAEA-RGK-1 reference materials from the International Atomic Energy Agency. Moska *et al.* (2021) provided a comprehensive description of the calibration procedure along the details on the laboratory equipment utilised. Typically, the counting time was set to 80 ks, with the sample mass of approximately 100 g. To calculate activity concentrations for the ^{238}U decay chain, the following gamma lines were used: 295.1 keV (^{214}Pb), 352.0 keV (^{214}Pb), 609.3 keV (^{214}Bi), 1120.3 keV (^{214}Bi), and 1764.5 keV (^{214}Bi). To determine the activity in the ^{232}Th decay chain, the gamma lines at 338.4 keV (^{228}Ac), 583.0 keV (^{208}Tl), 911.2 keV (^{228}Ac), and 2614.4 keV (^{208}Tl) were used. The ^{40}K activity concentration was obtain from the 1460.8 keV gamma line. In gamma analyses, the measurement results for ^{234}Th and their uncertainties did not allow for confirming the presence of radioactive disequilibrium in the ^{238}U decay series. However, the use of γBeaker measurement containers enabled the re-establishment of ^{222}Rn, thereby achieving radioactive equilibrium between ^{226}Ra and its decay products. Further information on the measurement procedures, as well as those concerning apparatus, calibration, and data analysis, can be found in another study (Wallbrink *et al.*, 2003). Comparative HRGS measurements were performed on the same samples.

3. Results and discussion

Fig. 7 displays the result of fitting spectra with the described method to an unknown sample alongside the retrieved pure spectra of uranium, thorium, and potassium. This figure effectively demonstrates the fitting's accuracy, as residuals shown in the insets, which compare the aligned results with the actual data.

In **Fig. 8**, it is shown how uncertainties vary with measurement time, both with and without inclusion of radionuclide correlations. The raw dose rates are determined assuming an infinite matrix. This calculation does not take into account water content, nor the *a*-value.

Table 2 compares the activity concentrations of ^{238}U, ^{232}Th, and ^{40}K as measured by the NaI:Tl system and HRGS for various samples. The results for 'JB' samples indicate a consistent measure of ^{238}U, ^{232}Th decay chain and ^{40}K activity concentrations across both systems within two standard deviations, except in the case of the ^{238}U JB8 sample where the consistency is noted at the 2σ level. Results of activity concentration of ^{238}U decay chain members measured with HRGS are provided in appendix **Table 1A**.

For the 'OSL/REP' samples differences, between NaI:Tl and HRGS are greater than for 'JB' samples, but still mostly within the 2σ level, indicating no statistical difference between these two methods. In investigated samples (**Table 2**) we did not observe a spectral shift during that would be visible in residuals during deconvolution.

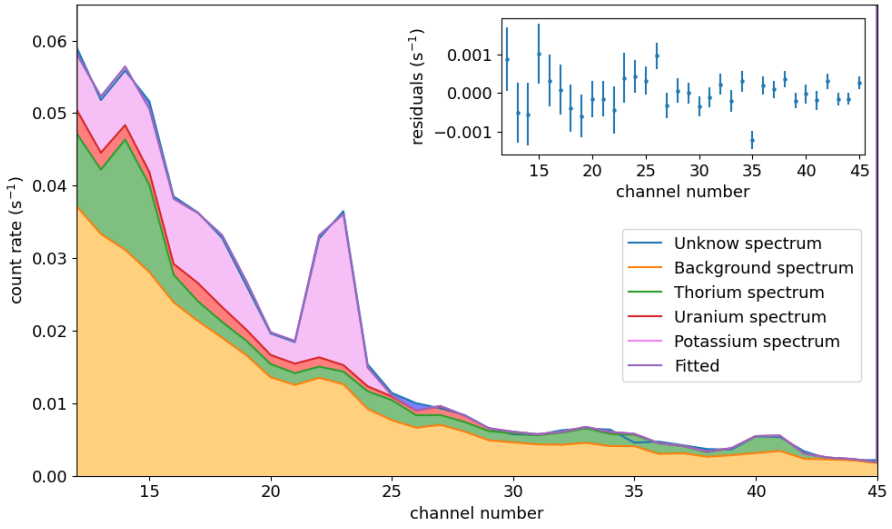

Fig. 7. *Example result of spectrum deconvolution. To an unknown spectrum (blue line), a fitted spectrum (purple line) is matched, from which background (orange line), thorium (green line), uranium (red line), potassium (pink line) are calculated. Residuals of the fitted spectra deconvolution are shown in inset.*

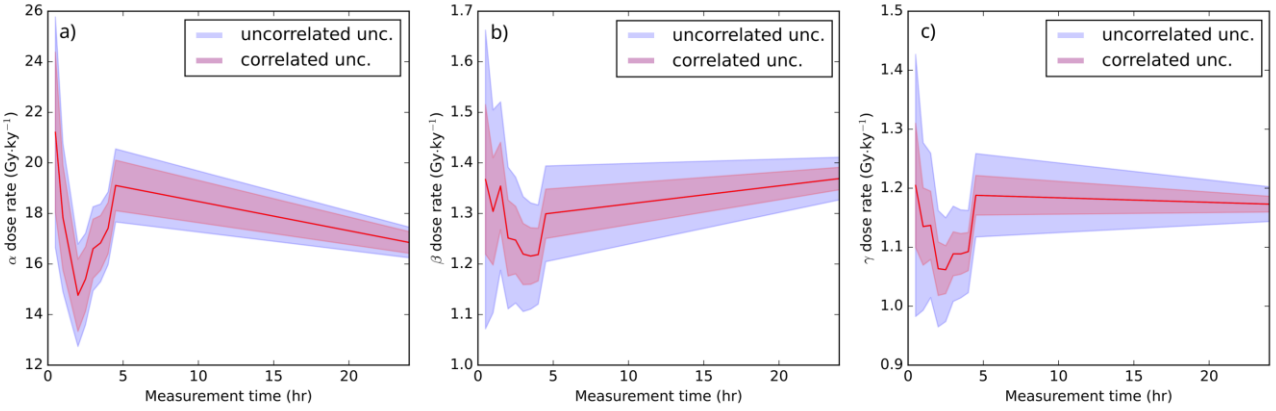

Fig. 8. *Raw α (a), β (b) and γ (c) dose rates value and uncertainties bands with and without accounting for correlations as a function of measurement time.*

Table 2. *Comparison of ^{238}U, ^{232}Th and ^{40}K activity concentrations achieved by using NaI:Tl scintillator and HRGS (high resolution gamma spectrometry). Uncertainties are expressed as 1σ.*

name	method	^{238}U activity concentration (Bq·kg^{-1})	^{232}Th activity concentration (Bq·kg^{-1})	^{40}K activity concentration (Bq·kg^{-1})
JB1	NaI:Tl	17.0 ± 2.4	32.3 ± 1.4	313 ± 11
	HRGS	16.73 ± 0.69	31.85 ± 0.74	324 ± 28
JB2	NaI:Tl	14.3 ± 2.4	35.8 ± 1.4	309 ± 11
	HRGS	17.87 ± 0.75	34.7 ± 1.2	317 ± 27
JB4	NaI:Tl	21.1 ± 2.5	53.1 ± 1.4	411 ± 12
	HRGS	20.69 ± 0.72	56.5 ± 1.8	424 ± 35
JB6	NaI:Tl	15.7 ± 2.5	48.7 ± 1.5	418 ± 12
	HRGS	20.86 ± 0.73	49.3 ± 1.6	424 ± 35
JB7	NaI:Tl	18.5 ± 2.3	35.5 ± 1.3	448 ± 12
	HRGS	21.25 ± 0.80	38.3 ± 1.3	462 ± 39
JB8	NaI:Tl	15.7 ± 2.4	39.6 ± 1.4	494 ± 12
	HRGS	22.91 ± 0.84	40.6 ± 1.4	501 ± 42
OSL/REP/1/1	NaI:Tl	21.4 ± 2.7	99.8 ± 1.7	46 ± 11
	HRGS	24.50 ± 0.80	98.1 ± 1.9	74.7 ± 7.6
OSL/REP/1/2	NaI:Tl	12.5 ± 2.0	11.1 ± 1.1	127.8 ± 9.0
	HRGS	14.70 ± 0.50	14.20 ± 0.70	154 ± 12
OSL/REP/1/3	NaI:Tl	25.9 ± 2.7	70.8 ± 1.7	272 ± 12
	HRGS	31.8 ± 1.0	73.4 ± 1.6	305 ± 24

In **Table 3**, the dose rates for various samples are provided. The calculation procedure described in Section 2.4. For the JB samples, α and β dose rates align closely within a 1σ level, whereas γ dose rate aligns at a 2σ level. This suggests that NaI:Tl scintillators are a viable alternative to HRGS. The table also compares results for Na:Tl scintillators, considering both scenarios: with and without radionuclide correlations (^{238}U, ^{232}Th, and ^{40}K). Accounting for these correlations generally reduces uncertainty, notably by up to 6% for JB samples and significant 35% for the γ dose rate of the OSL/REP/1/2 sample.

With μRate web app, variance-based sensitivity analysis was performed to calculate the Sobol indices (Saltelli *et al.*, 2010; Sobol, 2001). These indices quantify the extent to which each uncertain parameter contributes to the overall output variance. The software computes both the first-order sensitivity index and the total-effect index. To account for correlations among activity concentrations and other parameters, we grouped them together, treating them as multidimensional variables. This approach was inspired by Jacques *et al.* (2006).

Our sensitivity analysis performed on the samples yielded interesting findings. For example, for the JB2 sample, we observed a reduction in uncertainty associated with radionuclides when considering their correlations. Simultaneously, as radionuclide correlations were taken into account in dose rate calculations, other components contributing to dose rate uncertainty began to emerge as more significant factors. **Fig. 9** illustrates the decrease in both the first-order sensitivity index and the total-effect index when incorporating radionuclide correlations into dose rate calculations.

Table 3. *Comparison of α, β, and γ dose rates achieved by using NaI:Tl scintillator and HRGS, taking into account and excluding correlations in the case of NaI:Tl scintillator. Uncertainties are expressed as 1σ.*

name	method	α dose rate Gy·ky^{-1}	β dose rate Gy·ky^{-1}	γ dose rate Gy·ky^{-1}
JB1	NaI:Tl – correl.	0.041 ± 0.023	1.024 ± 0.064	0.648 ± 0.055
	NaI:Tl – uncorrel.	0.041 ± 0.023	1.024 ± 0.068	0.648 ± 0.059
	HRGS	0.040 ± 0.022	1.043 ± 0.089	0.648 ± 0.057
JB2	NaI:Tl – correl.	0.042 ± 0.023	1.010 ± 0.063	0.663 ± 0.056
	NaI:Tl – uncorrel.	0.042 ± 0.023	1.010 ± 0.066	0.663 ± 0.060
	HRGS	0.044 ± 0.024	1.052 ± 0.088	0.681 ± 0.060
JB4	NaI:Tl – correl.	0.062 ± 0.034	1.388 ± 0.084	0.951 ± 0.079
	NaI:Tl – uncorrel.	0.062 ± 0.034	1.388 ± 0.088	0.951 ± 0.082
	HRGS	0.064 ± 0.036	1.43 ± 0.12	0.992 ± 0.085
JB6	NaI:Tl – correl.	0.054 ± 0.030	1.339 ± 0.081	0.876 ± 0.071
	NaI:Tl – uncorrel.	0.054 ± 0.030	1.339 ± 0.084	0.876 ± 0.074
	HRGS	0.058 ± 0.032	1.40 ± 0.12	0.920 ± 0.079
JB7	NaI:Tl – correl.	0.045 ± 0.024	1.361 ± 0.083	0.779 ± 0.065
	NaI:Tl – uncorrel.	0.045 ± 0.025	1.361 ± 0.086	0.779 ± 0.069
	HRGS	0.049 ± 0.027	1.43 ± 0.12	0.834 ± 0.074
JB8	NaI:Tl – correl.	0.046 ± 0.025	1.466 ± 0.088	0.833 ± 0.068
	NaI:Tl – uncorrel.	0.046 ± 0.026	1.466 ± 0.091	0.833 ± 0.072
	HRGS	0.052 ± 0.029	1.55 ± 0.13	0.896 ± 0.080
OSL/REP/1/1	NaI:Tl – correl.	0.123 ± 0.063	0.795 ± 0.037	1.244 ± 0.042
	NaI:Tl – uncorrel.	0.123 ± 0.063	0.795 ± 0.043	1.244 ± 0.049
	HRGS	0.124 ± 0.063	0.877 ± 0.040	1.270 ± 0.045
OSL/REP/1/2	NaI:Tl – correl.	0.025 ± 0.013	0.476 ± 0.025	0.318 ± 0.018
	NaI:Tl – uncorrel.	0.025 ± 0.013	0.476 ± 0.032	0.318 ± 0.028
	HRGS	0.031 ± 0.016	0.575 ± 0.035	0.390 ± 0.017
OSL/REP/1/3	NaI:Tl – correl.	0.087 ± 0.044	1.075 ± 0.039	1.032 ± 0.032
	NaI:Tl – uncorrel.	0.087 ± 0.045	1.075 ± 0.044	1.032 ± 0.039
	HRGS	0.094 ± 0.049	1.200 ± 0.062	1.119 ± 0.038

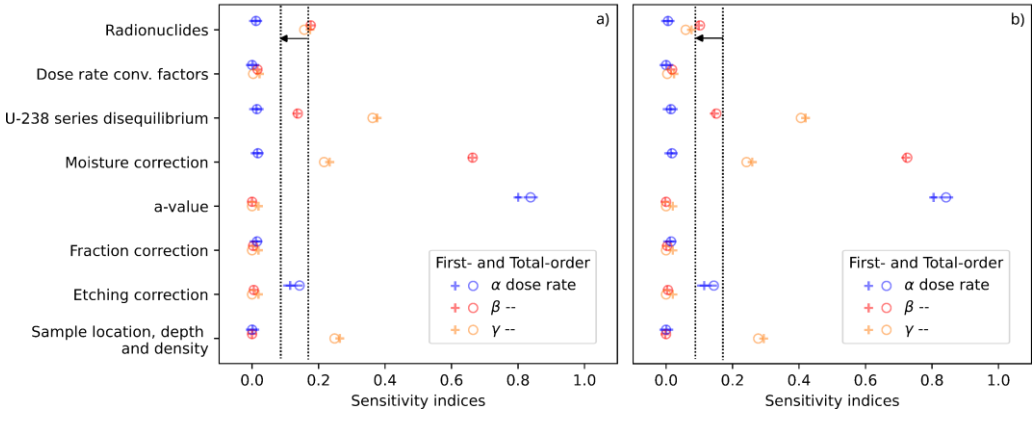

Fig. 9. *Sensitivity analysis of dose rates obtained from the JB2 sample for (a) uncorrelated and (b) correlated radionuclides using NaI:Tl. The dotted line illustrates the reduction of uncertainty components related with radionuclides.*

In our approach, multiple factors affect the precision and accuracy of radionuclide concentration determination and subsequent dose rate calculations. Notably, for brief measurement periods, such as a few minutes to hours, the software is prone to identifying multiple local minima, resulting in a range of possible solutions. This issue tends to resolve with longer measurement durations. This aspect is a more profound in classical net peak counts determination. Our calibration is based on IAEA-RGU-1 and IAEA-RGTh-1 reference materials, which are in a state of secular equilibrium. We operate under the assumption that our samples are nearly in this equilibrium state, expecting that our isolated uranium and thorium spectra will contribute accurately to our measured spectra. This assumption, however, may not be valid for all material types, as some environmental materials may be in radioactive disequilibrium (Bonczyk *et al.*, 2022; Méndez-Quintas *et al.*, 2019; Michalik *et al.*, 2020; Sakoda *et al.*, 2010). While

radioactive disequilibrium is infrequently mentioned in TCD literature, our method still holds potential applicability. Moreover, the type of material being analysed can suggest the likelihood of disequilibrium. The presence of disequilibrium not only shifts the results but also necessitates incorporating these variations into the dose rate calculation model (Degering and Degering, 2020).

The capability of our method to summing pure spectra into the measured spectrum indicates its utility as a potential tool in identifying certain disequilibrium types in materials. By inspecting the residuals from fitting processes and evaluating the goodness of fit, it might be possible to detect disequilibrium in samples. This, for a specific sample, can be an indicate the need for more comprehensive investigations using other techniques like HRGS, Instrumental Neutron Activation Analysis (INAA), or Inductively Coupled Plasma Mass Spectrometry (ICP-MS).

4. Conclusions

Our new method for analysing spectral data processes, fits, and isolates pure uranium, thorium, and potassium spectra (**Fig. 7**), providing accurate estimates of unknown radionuclides.

The NaI:Tl scintillator method presented here sufficiently measures radionuclide concentrations (**Table 2**) and dose rates (**Table 3**), with the results being in agreement with the HRGS results on the 2σ level. This new approach processes full spectra and allows for calibration with mixed standards. It includes correlation, reduces measurement time, and enhances efficiency (see **Fig. 8**) without compromising accuracy. **Fig. 9** demonstrates a notable reduction in the uncertainty associated with radionuclide measurements. Correlated uncertainties arising from radionuclides estimates are significantly lower than uncorrelated (**Figs 8, 9**), although other sources of uncertainty are more dominant (**Fig. 9**).

There are several advantages to this method. First, it allows the analysis of entire spectra, enabling the assessment of U, Th, and K estimates with shorter counting times. Second, it incorporates correlated uncertainties in dose rate calculations, slightly reducing the overall dose rate uncertainty. In principle, a similar approach can be used to calibrate the system for on-site measurements using calibration blocks. This would allow the estimation of not only gamma dose rates but also beta and alpha dose rates with relatively short counting times.

This method has promising applications in environmental activity concentration assessments and the dating of geological samples.

Acknowledgments

MG is pleased to acknowledge the Silesian University of Technology's funding of scientific associations as part of the "Excellence Initiative-Research University" program. We are thankful to Grzegorz Adamiec for his critical language corrections, contributing significantly to this manuscript.

Appendix A

Table 1A contains activities concentration measured of ^{238}U decay chain radionuclides measured with HRGS.

Table 1A. *Comparison of ^{238}U decay chain radionuclides measured with HRGS. Uncertainties are expressed as 1σ.*

name	^{214}Pb 295.1 keV (Bq·kg^{-1})	^{214}Pb 352.0 keV (Bq·kg^{-1})	^{214}Bi 609.3 keV (Bq·kg^{-1})	^{214}Bi 1120.3 keV (Bq·kg^{-1})	^{214}Bi 1764.5 keV (Bq·kg^{-1})	Weighted mean* (Bq·kg^{-1})
JB1	17.3 ± 1.4	17.1 ± 1.0	16.3 ± 1.1	15.9 ± 3.0	15.6 ± 2.7	16.73 ± 0.69
JB2	18.0 ± 1.5	17.7 ± 1.0	18.0 ± 1.3	16.2 ± 3.0	19.7 ± 3.1	17.87 ± 0.75
JB4	23.0 ± 1.5	20.3 ± 1.0	20.4 ± 1.1	18.5 ± 2.3	20.5 ± 2.3	20.69 ± 0.72
JB6	22.2 ± 1.4	21.0 ± 1.1	21.1 ± 1.2	18.4 ± 2.1	18.3 ± 2.2	20.86 ± 0.73
JB7	20.6 ± 1.5	20.9 ± 1.2	21.6 ± 1.3	18.6 ± 2.9	27.5 ± 3.0	21.25 ± 0.80
JB8	24.4 ± 1.7	23.1 ± 1.2	23.5 ± 1.3	18.5 ± 2.9	19.7 ± 2.7	22.91 ± 0.84
OSL/REP/1/1	24.04 ± 1.4	24.7 ± 1.4	24.9 ± 1.5	25.9 ± 2.9	22.3 ± 2.5	24.50 ± 0.80
OSL/REP/1/2	14.92 ± 0.89	14.32 ± 0.81	14.87 ± 0.89	13.9 ± 1.9	13.1 ± 1.7	14.70 ± 0.50
OSL/REP/1/3	33.1 ± 1.7	31.4 ± 1.6	30.9 ± 1.7	33.0 ± 3.1	34.3 ± 2.7	31.8 ± 1.0

** assumed as ^{238}U decay chain activity concentration*

References

Adamiec G, 2005a. OSL decay curves—relationship between single- and multiple-grain aliquots. *Radiation Measurements* 39(1): 63–75, DOI 10.1016/j.radmeas.2004.03.007.

Adamiec G, 2005b. Properties of the 360 and TL emissions of the '110°C peak' in fired quartz. *Radiation Measurements* 39(1): 105–110, DOI 10.1016/j.radmeas.2004.03.006.

Aitken MJ, 1985a. Alpha particle effectiveness: numerical relationship between systems. *Ancient TL* 3(3): 22–25, DOI 10.26034/la.atl.1985.095.

Aitken MJ, 1985b. *Thermoluminescence Dating*. Academic Press: London.

Aitken MJ and Xie J, 1990. Moisture correction for annual gamma dose. *Ancient TL* 8(2): 6–9, DOI 10.26034/la.atl.1990.157.

Arnold LJ, Duval M, Falguères C, Bahain J-J and Demuro M, 2012. Portable gamma spectrometry with cerium-doped lanthanum bromide scintillators: Suitability assessments for luminescence and electron spin resonance dating applications. *Radiation Measurements* 47(1): 6–18, DOI 10.1016/j.radmeas.2011.09.001.

Bejarano-Arias I, Van Wees RMJ, Alexanderson H, Janočko J and Perić ZM, 2023. Testing the Applicability of Quartz and Feldspar for Luminescence Dating of Pleistocene Alluvial Sediments in the Tatra Mountain Foothills, Slovakia. *Geochronometria* 50(1): 50–80, DOI 10.2478/geochr-2023-0002.

Bluszcz A and Adamiec G, 2006. Application of differential evolution to fitting OSL decay curves. *Radiation Measurements* 41(7–8): 886–891, DOI 10.1016/j.radmeas.2006.05.016.

Bonczyk M, 2018. Determination of 210 Pb concentration in NORM waste – An application of the transmission method for self-attenuation corrections for gamma-ray spectrometry. *Radiation Physics and Chemistry* 148: 1–4, DOI 10.1016/j.radphyschem.2018.02.011.

Bonczyk M, Chałupnik S, Wysocka M, Grygier A, Hildebrandt R and Tosheva Z, 2022. The Determination of Radon/Thoron Exhalation Rate in an Underground Coal Mine—Preliminary Results. *International Journal of Environmental Research and Public Health* 19(10): 6038, DOI 10.3390/ijerph19106038.

Branch MA, Coleman TF and Li Y, 1999. A Subspace, Interior, and Conjugate Gradient Method for Large-Scale Bound-Constrained Minimization Problems. *SIAM Journal on Scientific Computing* 21(1): 1–23, DOI 10.1137/S1064827595289108.

Brennan BJ, Lyons RG and Phillips SW, 1991. Attenuation of alpha particle track dose for spherical grains. *International Journal of Radiation Applications and Instrumentation. Part D. Nuclear Tracks and Radiation Measurements* 18(1–2): 249–253, DOI 10.1016/1359-0189(91)90119-3.

Brill D, Ageby L, Obert C, Hollerbach R, Duval M, Kolb T and Bartz M, 2022. Investigating the resetting of IRSL signals in beach cobbles and their potential for rock surface dating of marine terraces in Northern Chile. *Marine Geology* 443: 106692, DOI 10.1016/j.margeo.2021.106692.

Bu M, Murray AS, Kook M, Buylaert J-P and Thomsen KJ, 2021. The Application of Full Spectrum Analysis to NaI(Tl) Gamma Spectrometry for the Determination of Burial Dose Rates. *Geochronometria* 48(1): 161–170, DOI 10.2478/geochr-2020-0009.

Bu M, Murray AS, Kook M, Helsted LM, Buylaert J-P and Thomsen KJ, 2018. Characterisation of scintillator-based gamma spectrometers for determination of sample dose rate in OSL dating applications. *Radiation Measurements* 120: 253–259, DOI 10.1016/j.radmeas.2018.07.003.

Condori A, 2020. CNFreader, accessed 2023-12-01. https://github.com/Squawk322/CNFreader/.

Cresswell AJ, Carter J and Sanderson DCW, 2018. Dose rate conversion parameters: Assessment of nuclear data. *Radiation Measurements* 120: 195–201, DOI 10.1016/j.radmeas.2018.02.007.

Degering D and Degering A, 2020. Change is the only constant - time-dependent dose rates in luminescence dating. *Quaternary Geochronology* 58: 101074, DOI 10.1016/j.quageo.2020.101074.

Duval M and Arnold LJ, 2013. Field gamma dose-rate assessment in natural sedimentary contexts using LaBr3(Ce) and NaI(Tl) probes: A comparison between the "threshold" and "windows" techniques. *Applied Radiation and Isotopes* 74: 36–45, DOI 10.1016/j.apradiso.2012.12.006.

Ginter A, Moska P, Poręba G, Tudyka K, Szymak A and Szczurek G, 2022. Dates of Artifacts from Lusatian Urnfield Cemetery at Brzezie, Greater Poland. *Radiocarbon* 64(6): 1471–1482, DOI 10.1017/RDC.2022.70.

Guérin G, Mercier N, Nathan R, Adamiec G and Lefrais Y, 2012. On the use of the infinite matrix assumption and associated concepts: A critical review. *Radiation Measurements* 47(9): 778–785, DOI 10.1016/j.radmeas.2012.04.004.

Harris CR, Millman KJ, Van Der Walt SJ, Gommers R, Virtanen P, Cournapeau D, Wieser E, Taylor J, Berg S, Smith NJ, Kern R, Picus M, Hoyer S, Van Kerkwijk MH, Brett M, Haldane A, Del Río JF, Wiebe M, Peterson P, Gérard-Marchant P, Sheppard K, Reddy T, Weckesser W, Abbasi H, Gohlke C and Oliphant TE, 2020. Array programming with NumPy. *Nature* 585(7825): 357–362, DOI 10.1038/s41586-020-2649-2.

Hendriks PHGM, Limburg J and De Meijer RJ, 2001. Full-spectrum analysis of natural γ-ray spectra. *Journal of Environmental Radioactivity* 53(3): 365–380, DOI 10.1016/S0265-931X(00)00142-9.

Jacques J, Lavergne C and Devictor N, 2006. Sensitivity analysis in presence of model uncertainty and correlated inputs. *Reliability Engineering & System Safety* 91(10): 1126–1134, DOI 10.1016/j.ress.2005.11.047.

Kumar R, Frouin M, Gazack J and Schwenninger J-L, 2022. OxGamma: A MATLAB based application for the analysis of gamma-ray spectra. *Radiation Measurements* 154: 106761, DOI 10.1016/j.radmeas.2022.106761.

Lai ZP, Zöller L, Fuchs M and Brückner H, 2008. Alpha efficiency determination for OSL of quartz extracted from Chinese loess. *Radiation Measurements* 43(2–6): 767–770, DOI 10.1016/j.radmeas.2008.01.022.

Markkanen M and Arvela H, 1992. Radon Emanation from Soils. *Radiation Protection Dosimetry* 45(1–4): 269–272, DOI 10.1093/rpd/45.1-4.269.

Mauz B, Nolan PJ and Appleby PG, 2022. Technical note: Quantifying uranium-series disequilibrium in natural samples for dosimetric dating – Part 1: gamma spectrometry. *Geochronology* 4(1): 213–225, DOI 10.5194/gchron-4-213-2022.

Méndez-Quintas E, Demuro M, Arnold LJ, Duval M, Pérez-González A and Santonja M, 2019. Insights into the late stages of the Acheulean technocomplex of Western Iberia from the Arbo site (Galicia, Spain). *Journal of Archaeological Science: Reports* 27: 101934, DOI 10.1016/j.jasrep.2019.101934.

Mercier N and Falguères C, 2007. Field gamma dose-rate measurement with a NaI(Tl) detector: re-evaluation of the "threshold" technique. *Ancient TL* 25: 1–4, DOI 10.26034/la.atl.2007.400.

Michalik B, Wysocka M, Bonczyk M, Samolej K and Chmielewska I, 2020. Long term behaviour of radium rich deposits in a lake ecosystem. *Journal of Environmental Radioactivity* 222: 106349, DOI 10.1016/j.jenvrad.2020.106349.

Moska P, Bluszcz A, Poręba G, Tudyka K, Adamiec G, Szymak A and Przybyła A, 2021. Luminescence Dating Procedures at the Gliwice Luminescence Dating Laboratory. *Geochronometria* 48(1): 1–15, DOI 10.2478/geochr-2021-0001.

Moska P, Jary Z, Adamiec G and Bluszcz A, 2019. Chronostratigraphy of a loess-palaeosol sequence in Biały Kościół, Poland using OSL and

radiocarbon dating. *Quaternary International* 502: 4–17, DOI 10.1016/j.quaint.2018.05.024.

Murray A, Buylaert J-P and Thiel C, 2015. A luminescence dating intercomparison based on a Danish beach-ridge sand. *Radiation Measurements* 81: 32–38, DOI 10.1016/j.radmeas.2015.02.012.

Murray AS, Helsted LM, Autzen M, Jain M and Buylaert JP, 2018. Measurement of natural radioactivity: Calibration and performance of a high-resolution gamma spectrometry facility. *Radiation Measurements* 120: 215–220, DOI 10.1016/j.radmeas.2018.04.006.

Panin A, Adamiec G, Buylaert J-P, Matlakhova E, Moska P and Novenko E, 2017. Two Late Pleistocene climate-driven incision/aggradation rhythms in the middle Dnieper River basin, west-central Russian Plain. *Quaternary Science Reviews* 166: 266–288, DOI 10.1016/j.quascirev.2016.12.002.

Pawełczyk F, Bolik A, Błachut B, Kamińska A, Opała-Owczarek M, Malik I, Wojcik M, Zakrzewska Z, Pawlak Z and Poręba G, 2023. Development of Chronology for Historical Mining Shaft Remains in the Vicinity of Tarnowskie Góry Based on Radiocarbon, Luminescence and Dendrochronological Dating. *Geochronometria* 50(1): 81–90, DOI 10.2478/geochr-2023-0004.

Perić ZM, Stevens T, Obreht I, Hambach U, Lehmkuhl F and Marković SB, 2022. Detailed luminescence dating of dust mass accumulation rates over the last two glacial-interglacial cycles from the Irig loess-palaeosol sequence, Carpathian Basin. *Global and Planetary Change* 215: 103895, DOI 10.1016/j.gloplacha.2022.103895.

Poręba G, Tudyka K, Walencik-Łata A and Kolarczyk A, 2020. Bias in 238U decay chain members measured by γ-ray spectrometry due to 222Rn leakage. *Applied Radiation and Isotopes* 156: 108945, DOI 10.1016/j.apradiso.2019.108945.

Rhodes EJ and Schwenninger J-L, 2007. Dose rates and radioisotope concentrations in the concrete calibration blocks at Oxford. Ancient TL 25: 5–8, DOI 10.26034/la.atl.2007.401.

Rocznik J, Pluta J, Tudyka K, Poręba G and Szymak A, 2023. A new fast screening method for estimating building materials hazard indices with correlated inputs. *Journal of Radioanalytical and Nuclear Chemistry* 332(12): 4889– 4896, DOI 10.1007/s10967-023-09197-5.

Sakoda A, Ishimori Y and Yamaoka K, 2011. A comprehensive review of radon emanation measurements for mineral, rock, soil, mill tailing and fly ash. *Applied Radiation and Isotopes* 69(10): 1422–1435, DOI 10.1016/j.apradiso.2011.06.009.

Sakoda A, Nishiyama Y, Hanamoto K, Ishimori Y, Yamamoto Y, Kataoka T, Kawabe A and Yamaoka K, 2010. Differences of natural radioactivity and radon emanation fraction among constituent minerals of rock or soil. *Applied Radiation and Isotopes* 68(6): 1180–1184, DOI 10.1016/j.apradiso.2009.12.036.

Saltelli A, Annoni P, Azzini I, Campolongo F, Ratto M and Tarantola S, 2010. Variance based sensitivity analysis of model output. Design and estimator for the total sensitivity index. *Computer Physics Communications* 181(2): 259–270, DOI 10.1016/j.cpc.2009.09.018.

Seo BK, Lee KY, Yoon YY and Lee DW, 2001. Direct and precise determination of environmental radionuclides in solid materials using a modified Marinelli beaker and a HPGe detector. *Fresenius' Journal of Analytical Chemistry* 370(2–3): 264–269, DOI 10.1007/s002160000695.

Sobol IM, 2001. Global sensitivity indices for nonlinear mathematical models and their Monte Carlo estimates. *Mathematics and Computers in Simulation* 55(1): 271–280, DOI 10.1016/S0378-4754(00)00270-6.

Sontag-González M, Li B, O'Gorman K, Sutikna T, Jatmiko, Jacobs Z and Roberts RG, 2021. Establishing a pIRIR procedure for De determination of composite mineral grains from volcanic terranes: A case study of sediments from Liang Bua, Indonesia. *Quaternary Geochronology* 65: 101181, DOI 10.1016/j.quageo.2021.101181.

Tudyka K, Bluszcz A, Poręba G, Miłosz S, Adamiec G, Kolarczyk A, Kolb T, Lomax J and Fuchs M, 2020. Increased dose rate precision in combined α and β counting in the μDose system - a probabilistic approach to data analysis. *Radiation Measurements* 134 106310, DOI 10.1016/j.radmeas.2020.106310.

Tudyka K, Koruszowic M, Osadnik R, Adamiec G, Moska P, Szymak A, Bluszcz A, Zhang J, Kolb T and Poręba G, 2023. μRate: An online dose rate calculator for trapped charge dating. *Archaeometry* 65(2): 423–443, DOI 10.1111/arcm.12828.

Tudyka K, Poręba G, Szymak A, Rocznik J, Pluta J, Schüler T, Kolb T and Murray A, 2021. Systematic error in 238U decay chain radionuclides measurements due to 222Rn emanation from reference materials. *Measurement* 184: 109893, DOI 10.1016/j.measurement.2021.109893.

Virtanen P, Gommers R, Oliphant TE, Haberland M, Reddy T, Cournapeau D, Burovski E, Peterson P, Weckesser W, Bright J, Van Der Walt SJ, Brett M, Wilson J, Millman KJ, Mayorov N, Nelson ARJ, Jones E, Kern R, Larson E, Carey CJ, Polat İ, Feng Y, Moore EW, VanderPlas J, Laxalde D, Perktold J, Cimrman R, Henriksen I, Quintero EA, Harris CR, Archibald AM, Ribeiro AH, Pedregosa F, Van Mulbregt P, SciPy 1.0 Contributors, Vijaykumar A, Bardelli AP, Rothberg A, Hilboll A, Kloeckner A, Scopatz A, Lee A, Rokem A, Woods CN, Fulton C, Masson C, Häggström C, Fitzgerald C, Nicholson DA, Hagen DR, Pasechnik DV, Olivetti E, Martin E, Wieser E, Silva F, Lenders F, Wilhelm F, Young G, Price GA, Ingold G-L, Allen GE, Lee GR, Audren H, Probst I, Dietrich JP, Silterra J, Webber JT, Slavič J, Nothman J, Buchner J, Kulick J, Schönberger JL, De Miranda Cardoso JV, Reimer J, Harrington J, Rodríguez JLC, Nunez-Iglesias J, Kuczynski J, Tritz K, Thoma M, Newville M, Kümmerer M, Bolingbroke M, Tartre M, Pak M, Smith NJ, Nowaczyk N, Shebanov N, Pavlyk O, Brodtkorb PA, Lee P, McGibbon RT, Feldbauer R, Lewis S, Tygier S, Sievert S, Vigna S, Peterson S, More S, Pudlik T, Oshima T, Pingel TJ, Robitaille TP, Spura T, Jones TR, Cera T, Leslie T, Zito T, Krauss T, Upadhyay U, Halchenko YO and Vázquez-Baeza Y, 2020. SciPy 1.0: fundamental algorithms for scientific computing in Python. *Nature Methods* 17(3): 261–272, DOI 10.1038/s41592-019-0686-2.

Vugrin KW, Swiler LP, Roberts RM, Stucky-Mack NJ and Sullivan SP, 2007. Confidence region estimation techniques for nonlinear regression in groundwater flow: Three case studies. *Water Resources Research* 43(3): 2005WR004804, DOI 10.1029/2005WR004804.

Wallbrink PJ, Walling DE and He Q, 2003. Radionuclide Measurement Using HPGe Gamma Spectrometry. In: Zapata F (ed) *Handbook for the Assessment of Soil Erosion and Sedimentation Using Environmental Radionuclides*. Kluwer Academic Publishers: Dordrecht, 67–96, DOI 10.1007/0-306-48054-9_5.